

www.aem-journal.com

# Slippery Liquid-Infused Porous Surface on Metal Material with Excellent Ice Resistance Fabricated by Femtosecond Bessel Laser

Jialiang Zhang, Qing Yang, Yang Cheng, Zheng Fang, Xun Hou, and Feng Chen\*

Slippery liquid-infused porous surface (SLIPS) has shown great application prospects because of the great liquid repellency and ice resistance. However, there are a few types of research on different metal material to fabricate SLIPS. Here, a simple and effective method is developed on a stainless steel surface to manufacture microporous structure by femtosecond Bessel laser beam direct induce. By fluoroalkylsilane modification and infusing lubricant, SLIPS is successfully obtained. The ice restraint properties of the SLIPS are studied, including the characterization of icing delay and ice-adhesion strength, which significantly increase the icing-delay time and reduce the ice-adhesion strength. Moreover, SLIPS exhibits great durability after hydraulic pressure, salt fog, high-, and low-temperature cycle. Based on this method, SLIPS can be produced on different metal substrates including Al, Zn, Ti, Cu with excellent liquid resistance and anti-icing property, which greatly expand the application of SLIPS in the field of ice resistance.

1. Introduction

Many kinds of outdoor infrastructure based on metal material will inevitably be threatened by snowing and icing in winter and cold areas. The formation and accumulation of ice on the surface of power lines and its tower,<sup>[1]</sup> aircraft,<sup>[2]</sup> offshore oil platforms,<sup>[3]</sup> wind turbines,<sup>[4]</sup> etc. have been seriously affected the normal operation of these facilities and cause disasters sometimes.<sup>[5,6]</sup> For example, the extreme weather that took place in southern China in 2008 led to ice accretion on power facilities resulting in 151.6 billion RMB in direct economic losses.<sup>[7,8]</sup> Preventing icing accumulation on exposed surfaces is a serious subject around the world. Conventional methods for removing ice or inhibiting icing, such as

J. Zhang, X. Hou, F. Chen
State Key Laboratory for Manufacturing System Engineering and Shaanxi
Key Laboratory of Photonics Technology for Information
School of Electronics & Information Engineering
Xi'an Jiaotong University
Xi'an 710049, P. R. China
E-mail: chenfeng@mail.xjtu.edu.cn

Q. Yang, Y. Cheng, Z. Fang School of Mechanical Engineering Xi'an Jiaotong University Xi'an 710049, P. R. China

The ORCID identification number(s) for the author(s) of this article can be found under https://doi.org/10.1002/adem.202101738.

DOI: 10.1002/adem.202101738

Adv. Eng. Mater. 2022, 24, 2101738

heating, mechanical de-icing, releasing antiicing agents, are either inefficient or high energy consumption. [9,10]

In recent years, the passive anti-icing surface material has been developed by many researchers including superhydrophobic surfaces and slippery liquid infused porous surfaces. Superhydrophobic surface (SHS) inspired by lotus leaves, [11-16] possessing extraordinary water resistance, which could be applied in the field of anti-icing by diminishing contact area between the solid and liquid.[17-28] Wang fabricated a superhydrophobic surface on stainless steel via laser direct microprocessing, which presents excellent icing-delay ability. [29] However, due to the instability of the air layer on SHS, the surfaces could be easily lost superhydrophobic performance with long-term use in a complex

environment, and became more difficult to remove ice off the surface. [30-34] Recently, SLIPS inspired by the nepenthes plant has attracted great attention of researchers due to their distinguished liquid repellency and ice restraint performance.<sup>[35,36]</sup> Unlike the unstable air layer of the SHS, SLIPS owns a stable lubricant layer between the surface textures and the liquid, exhibiting a better performance in dynamic liquid repellence. Cong Li presented network surface structures that firmly locked and stored the lubricant, leading to an efficient anti-icing performance by electrochemical etching and hydrothermal process. [37] Sumit Barthwal designed a slippery oil-infused poly-dimethylsiloxane (PDMS) coating on a structured Al surface with low iceadhesion properties. [38] The anti-icing performance has been realized on different metal substrates by directly fabricating SLIPS on a specific metal substrate or producing polymer SLIPS coatings on metal substrates.<sup>[39–42]</sup> However, in the existing researches, different metal substrates are required for different anti-icing applications, and the methods used are specific to directly achieve SLIPS on the corresponding metal substrate. Besides, when the ambient temperature changes dramatically, the bonding strength is seriously affected by the large difference in thermal expansion coefficient between the polymer SLIPS coating and the metal substrate. These factors greatly limit the practical application of anti-icing surfaces. [43] The demand for anti-icing surfaces is needed in extremely harsh natural environments in practical applications, which are accompanied by ultrahigh humidity, ultralow temperature, alternation of high temperature, and low temperature with seasonal changes.

www.advancedsciencenews.com

www.aem-journal.com

15272648, 2022, 10, Downloaded from https://adatanced.onlinelibrary.wiley.com/doi/10.1002/adem.202101738 by CAS-XIAN INSTITUTION OPTICS PRECISION MECHANICS, Wiley Online Library on [1011/2025], See the Terms and Conditions (https://onlinelibrary.wiley.com/terms-and-conditions) on Wiley Online Library for rules of use, eQ. Aarticles are governed by the applicable Ceatwice Commons License

In this article, the microporous structure can be directly induced on stainless steel substrate by using a femtosecond Bessel laser beam. After further fluoroalkylsilane modification to lower the surface energy and infusing with lubricant oil, the SLIPS was successfully fabricated. SLIPS has great liquid resistance, and the droplets can slide away naturally with a small tilt angle. The ice restraint properties of the SLIPS were studied by characterization of icing delay and ice-adhesion strength. The ice-delay time of SLIPS was extended by 21.5% and 43.3% compared to SHS and untreated surface at a temperature of -30 °C, and the ice-adhesion strength can remain below 15 kPa after repeated numbers of cycles. Besides, the SLIPS can effectively maintain water repellency during various harsh environments such as hydraulic pressure, salt fog, high- and low-temperature cycle, and scratches. Furthermore, this method could be applied to construct porous structures and realize SLIPS on different kinds of metal materials (including stainless steel, Al, Zn, Ti, Cu), which shows excellent liquid repellency and ice-adhesion as well.

# 2. Results and Discussion

# 2.1. Fabrication of the SLIPS and Wettability of the SLIPS

The porous microstructure plays a key role in storing lubricating oil in the formation of the SLIPS. Compared to other methods in fabricating porous structure, the femtosecond laser has many advantages of high precision processing, strong controllability because of its ultrashort pulse width, and ultrahigh peak energy. Herein, the original Gaussian laser beam was spatially shaped into a Bessel laser beam through an axicon lens, using a femtosecond Bessel laser to produce porous morphology on the stainless steel surface. The microfabrication system based on the Bessel laser beam is shown in Figure 1a. The femtosecond laser with the traditional Gaussian profile was generated from a fiber laser device with a high frequency of 5 MHz, wavelength of 1030 nm. Since the energy center diameter of the Gaussian beam is larger than that of the Bessel beam, the Bessel laser beam is shaped by the original Gaussian beam through a conical lens. Then, the Bessel beam passes through the lens, the mirror, and the microscopic objective lens, in turn, to focus on the surface of stainless steel, the core diameter of the Bessel beam is compressed to about  $1.8\,\mu m.^{[44]}$  When the femtosecond Bessel laser is processed on the stainless steel sample, a large number of free electrons on the sample surface absorb the laser energy, thus reaching a high energy state and breaking the original equilibrium state of the sample surface. To regain the thermal equilibrium state, the high-energy electrons interact with the adjacent lattice through photoelectric coupling, which also leads to the increase of lattice temperature. When the lattice temperature is higher than the phase explosion temperature, the stainless steel undergoes a strong plasma jet process and thus forms a porous structure. The moving platform of the sample is matched with the selected frequency of the laser, which means the ablation of the laser at a fixed distance on the surface of the sample to form micropores. According to this mechanism, after selecting appropriate laser parameters and processing parameters, uniform and dense porous structures can be induced on the sample surface. As shown in Figure 1b,c, the microporous spreading on the substrate surface is very uniform and dense with every single hole's diameter around 2  $\mu m$ . According to the scanning electron microscope (SEM) image Figure 1b,c, the fill ratio of micro-holes on the surface reaches around 46%, which means it can store plenty of lubricant oil and lock it with great bound.

There are several steps to fabricate SLIPSs as shown in Figure 1d. First, the metal samples were polished with sandpaper until reached a high flatness. Second, the femtosecond Bessel beam laser was used to induce the porous microstructure on the substrate surface. After that, modification of porous samples with fluoroslkysilane to reduce the surface energy. Then, silicone oil was infused over the slightly inclined samples until the oil fully fills the whole micropores. The untreated stainless steel is hydrophilic. A water droplet (volume about 7 µL) on the stainless steel surface had a water contact angle (WCA) of 69.46° (Figure 1e). After the sample induced microporous structure by femtosecond Bessel laser, the WCA of the sample is 66.80° (Figure 1f) shows the surface energy does not change by laser ablation. After the fluroalkysilane decorated the sample with a microporous structure surface, a superhydrophobic sample was created, the reason is that fluroalkysilane greatly lowers the surface energy with the WCA of 153.25° (Figure 1g). Due to the extremely low surface energy of the decorated sample surface, the lubricant can easily enter the microporous structure under capillary force. Thus, the SLIPS was fabricated by infusing the silicone oil onto the surfaces, the silicon oil formed a stable lubricating film on the sample with a WCA of 102.25° (Figure 1h). The microporous structure has a strong binding force with lubricant, showing excellent liquid resistance. The water drop can easily slide away at a small tilt angle of SLIPS, Figure 1i shows the sliding process of a water droplet (volume about 7 µL) on the as-prepared SLIPS with a tilt angle of 4°. The results indicate that the SLIPS has excellent repellency to liquid.

The liquid resistance of stainless steel SLIPS with different droplet sizes was studied, including the static WCA and the sliding velocity on the  $10^\circ$  slope. As shown in Figure 2, the WCA slightly decreases with the increase of droplet volume from  $97^\circ$  at  $5\,\mu L$  to  $89^\circ$  at  $50\,\mu L$ . The sliding speed of the droplet on the  $10^\circ$  slope of SLIPS increases with the increase of the droplet volume, because the larger the droplet volume is, the larger the component of the droplet gravity on the SLIPS is, and the faster the droplet sliding on the SLIPS is. The sliding process was exhibited in Figure S1, Supporting Information, When the droplets are very tiny, they can also slide off SLIPS by their own gravity. The results indicate that the liquid resistance of the SLIPS is very stable, and it is not affected by the droplet size.

### 2.2. Ice Restraint Performance

The SLIPS ice restraint property was characterized by the ice-delay test and ice adhesion test. The water droplet of  $100\,\mu L$  was dropped on different surfaces, then placed in a cryogenic chamber at minus  $30\,^{\circ}C.$  Herein, the icing delay time was defined as the time span from when the sample with droplet was placed in the cryogenic chamber to that when the droplet is frozen completely. The icing process was pictured through

15272648, 2022, 10, Downloaded from https:

xxm/doi/10.1002/adem.202101738 by CAS-XIAN INSTITUTION OPTICS PRECISION MECHANICS, Wiley Online Library on [10/11/2025]. See the Terms

nditions) on Wiley Online Library for rules of use; OA articles are

governed by the applicable Creative Commons License

www.aem-journal.com

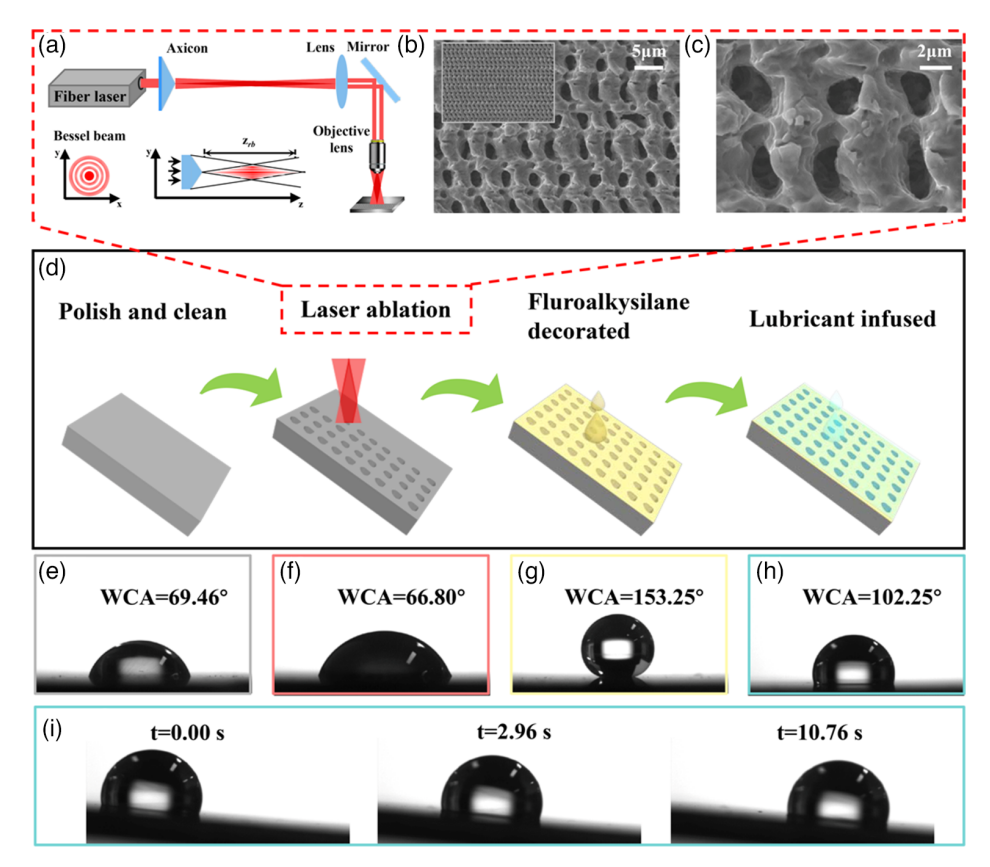


Figure 1. Fabrication of microporous structure on the stainless steel by femtosecond Bessel laser beam processing. a) Processing system of the microporous structure by Bessel laser beam through an axicon. b,c) Surface morphology of the stainless steel after being processed by femtosecond Bessel laser. d) Process of the slippery liquid-infused porous surface (SLIPS) on the stainless steel based on the microporous that femtosecond laser ablation. e–h) Water droplets on different stainless steel substrates: e) the intrinsic stainless steel, f) the laser-ablated microporous structure, g) the fluroalkysilane decorated microporous surface, h) SLIPS. i) Sliding process of a water droplet on the SLIPS with a tilted angle of 4°.

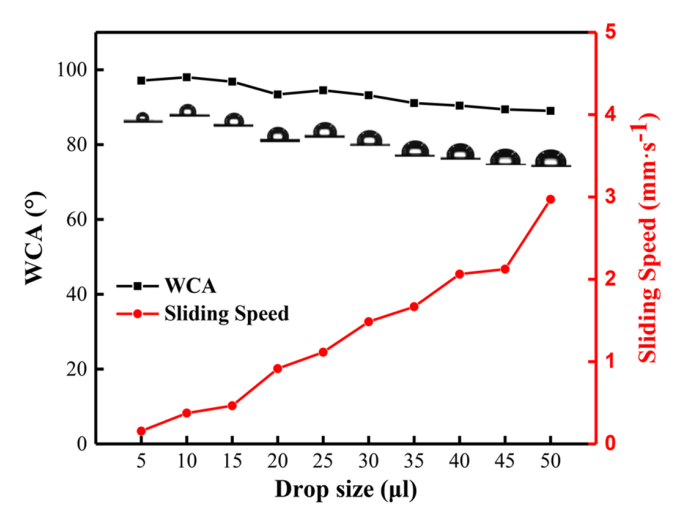


Figure 2. Water contact angle (WCA) and sliding speed on SLIPS of different droplet sizes.

the observation window of the cryogenic chamber. Three samples of icing-delay time were recorded and compared, which are untreated surface of stainless steel, the SHS of stainless steel,

the SLIPS of stainless steel, respectively. According to the ice-delay results shown in **Figure 3**a, the SLIPS own the longest ice-delay time of 247 s at the temperature of  $-30\,^{\circ}$ C, longer than SHS of 194 s and the untreated surface of 140 s. Compared to SHS and untreated surface, the ice-delay time of SLIPS was extended by 21.5% and 43.3%. The reason is that SLIPS owns an extra thickness film of lubricant, which obstructs the heat exchange between the cold substrate and the droplet and prolongs the freezing time.

The ice adhesion strength was tested on different samples for assessing the ice-restraint property. The ice formation was in  $a-30\,^{\circ}\text{C}$  cryogenic chamber for at least 7 h with deionized water 1 mL in a colorimetric dish reverse on the sample surface. Figure 3b gives ice adhesion tests results on the sample of untreated surface, SHS and SLIPS, respectively, which can be seen that SHS and SLIPS are able to reduce the adhesion strength of ice. SHS reduced the ice adhesion strength because of the superhydrophobic property of the sample that was decorated by fluroalkysilane, which has an air layer that reduced the adhesion strength between sample and water. However, the result of SHS surface is very much unstable with the increase of testing numbers, the reason is that SHS will lose its characteristics in humid and cold environments. Besides, the bubble could

15272648, 2022, 10, Downloaded from https://advanced.

online library, wiley, com/doi/10.1002/adem.202101738 by CAS-XIAN INSTITUTION OPTICS PRECISION MECHANICS, Wiley Online Library on [10/11/2025]. See the Terms and Conditions (https://online library.wiley.com/terms

-and-conditions) on Wiley Online Library for rules of use; OA articles are governed by the applicable Creative Commons License

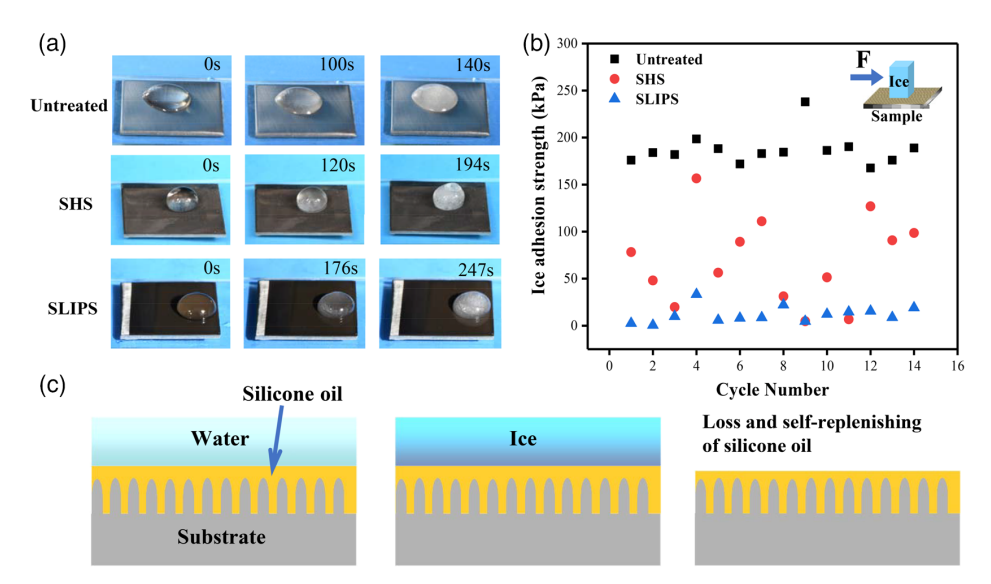


Figure 3. a) Icing delay time of untreated, superhydrophobic surface (SHS), and SLIPS surface. b) Ice adhesion tests result on the sample of untreated, SHS and SLIPS. c) Schematic of ice formation on SLIPS and ice removed from SLIPS.

be observed continuously appearing from the contact surface between SHS and liquid during the icing process, then rising to the liquid surface. This is due to the instability of the air layer stored in SHS, the bubble may be frozen on the interface between SHS and liquid during the icing process, which will cause uncertainty about the contact area between ice and SHS, then affects the ice adhesion strength. While the SLIPS reduced the ice shear strength by nearly two orders of magnitude relative to the untreated stainless steel sample. As we can see in the schematic diagram of water freezing on the SLIPS (Figure 3c), most of the lubricant oil was stored and locked in a microporous structure, the rest lubricant oil existed on the surface to form an ultrathin layer, which separates the water from the substrate and makes the nucleation of ice occur at the water/ oil interface. The results of SLIPS ice adhesion strength were below 15 kPa after 15 cycles of the tests. The reason is that the uniform and dense microporous structure with great adhesion to the lubricant, which makes it difficult for SLIPS to lose lubricant. However, with the increase of cycles, the SLIPS will reduce its performance due to the loss of lubricant. The solution is to directly drop the new lubricating oil on the surface to restore its liquid resistance and ice resistance. This is because the lubricating oil in the micropore is very difficult to lose, and the newly dropped lubricating oil can quickly combine with the lubricating oil in the micropore to form a new lubricating liquid thin layer.

### 2.3. Durability of SLIPS

To demonstrate the durability of the developed SLIPS, a series stability tests were conducted including hydraulic pressure test, salt fog test, high and low (H&L) temperature cycle, and mechanical durability, respectively. The hydraulic pressure test was carried out by putting the SLIPS in a visible hydraulic testing machine with a parameter of 30 m depth hydraulic pressure for 3 days. The salt fog test was processed SLIPS sample was

placed at a slope with an angle of 45° in a condition of 5 wt% NaCl fog at 35 °C for 2 days by using a salt fog test machine. The H&L temperature cycle was performed in the constant temperature and humidity test chamber, the SLIPS was placed in the chamber suffering the change of the temperature in sequence for 3 times cycles, in which the highest temperature was 130 °C of 3 h, lowest temperature was -30 °C of 3 h. As for the mechanical test, the SLIPS is scratched directly with a knife several times. The sliding speed of water drops of 7 µL on a 10° slope was contrasted after different stability tests to measure the stability of the SLIPS, sliding speed of each sample is measured three times, and averaged as shown in Figure 4a, which also exhibited the corresponding post-test SLIPS sample above the sliding speed. According to the results in Figure 4a, the sliding speeds are  $0.534, 0.404, 0.467, 0.424 \,\mathrm{mm \, s}^{-1}$  after experiencing hydraulic pressure, salt fog, H&L temperature cycle, scratch, respectively. It is obvious that the sliding speed was scarcely changed within the range of 0.02 mm s<sup>-1</sup> after different stability tests, which indicates that the SLIPS we prepared owns great stability to suffer many harsh environments. The sliding speed decreases the most after the salt fog test was 0.404 mm s<sup>-1</sup>, which is also an acceptable range. The reason is that the salt fog continuously condenses on the SLIPS into drops, these drops' volume grows along with time delay and will contact drops adjacent became bigger drops and slide down the sample, which would take away the lubricant slightly. However, the slippery property still exists after 2 days salt fog test, even though the SLIPS cannot slide down the  $10^{\circ}$  slope when the drops' volume was 7  $\mu$ L, while the volume of the droplet is big enough, it will still slide away. As for other tests, the SLIPS maintains great water repellency. Figure 4b shows the sliding process after different stability tests, the sliding distance is 6.2 mm. These results are from the strong junction between the porous structure and lubricant, on the one hand, the porous structure is tightly bonded with lubricant oil, on the other hand, the porous structure can store the lubricant oil so that the surface loss of lubricant oil can be replenished.

15272648, 2022, 10, Downloaded from https:

online library. wiley.com/doi/10.1002/adem.202101738 by CAS-XIAN INSTITUTION OPTICS PRECISION MECHANICS, Wiley Online Library on [10/11/2025]. See the Terms

on Wiley Online Library for rules of use; OA

governed by the applicable Creative Commons License

www.aem-journal.com

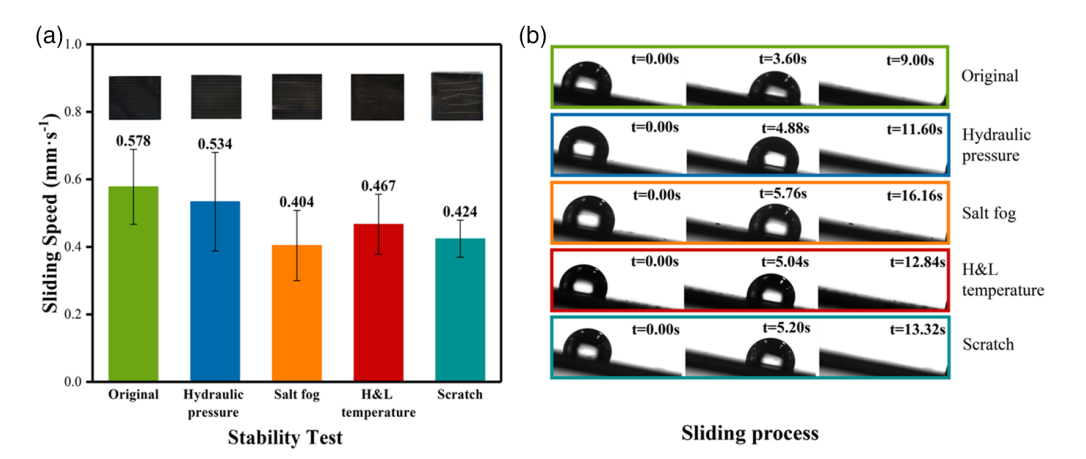


Figure 4. Stability test. a) Sliding speed of water drop of 7 μL on SLIPS with 10° inclined. b) Sliding process after different stability tests.

# 2.4. Universality of the Metal SLIPS Fabrication Method

The femtosecond Bessel beam laser ablation can be applied to various types of metal materials to induce microporous structure, and furtherly fabricate SLIPS. As shown in Figure 5, the microporous structure could be induced on Al, Zn, Ti, Cu, by using the same method and slightly adjusting the laser ablation parameters. According to Figure 4, the structural porosity of the microporous Al, Zn, Ti, Cu was able to estimate about 52.3%, 47.3%, 45.4%, 45.4% respectively. The microporous on different substrates are of great benefit to store and lock lubricant. The processing parameters for each metal are as follows: the scanning speed is  $12 \text{ mm s}^{-1}$ , the select-frequency is 3 kHz, the duty ratio is 25%, the original laser power is 2.2 W for Al substrate; the scanning speed is 15 mm s<sup>-1</sup>, the select-frequency is 2 kHz, the duty ratio is 15%, the original laser power is 1.63 W for Zn; the scanning speed is 12 mm s<sup>-1</sup>, the select-frequency is 2 kHz, the duty ratio is 20%, the original laser power is 2.9 W for Ti; the scanning speed is 10 mm s<sup>-1</sup>, the select-frequency is 2 kHz, the duty ratio is 30%, the original laser power is 4.5 W for Cu. With further low surface energy modification and infusing lubricant, we can obtain SLIPSs on different metal substrates. Then, the water repellency and ice adhesion performance were characterized as well, as shown in Figure 6. The WCA was measured at three points on each sample, three times on each point. The average WCA was shown at the red point in Figure 6a. The results of WCA and sliding speed indicate that the SLIPS on different metal materials prepared by this method have distinguished liquid resistance. The WCAs of SLIPS on the substrate of Al, Zn, Ti, Cu are 102.3°, 100.125°, 100.5°, 94.75°, respectively. The sliding speed of different SLIPS on a 10° slope with a water volume of about 7 µL was tested as well, the value of

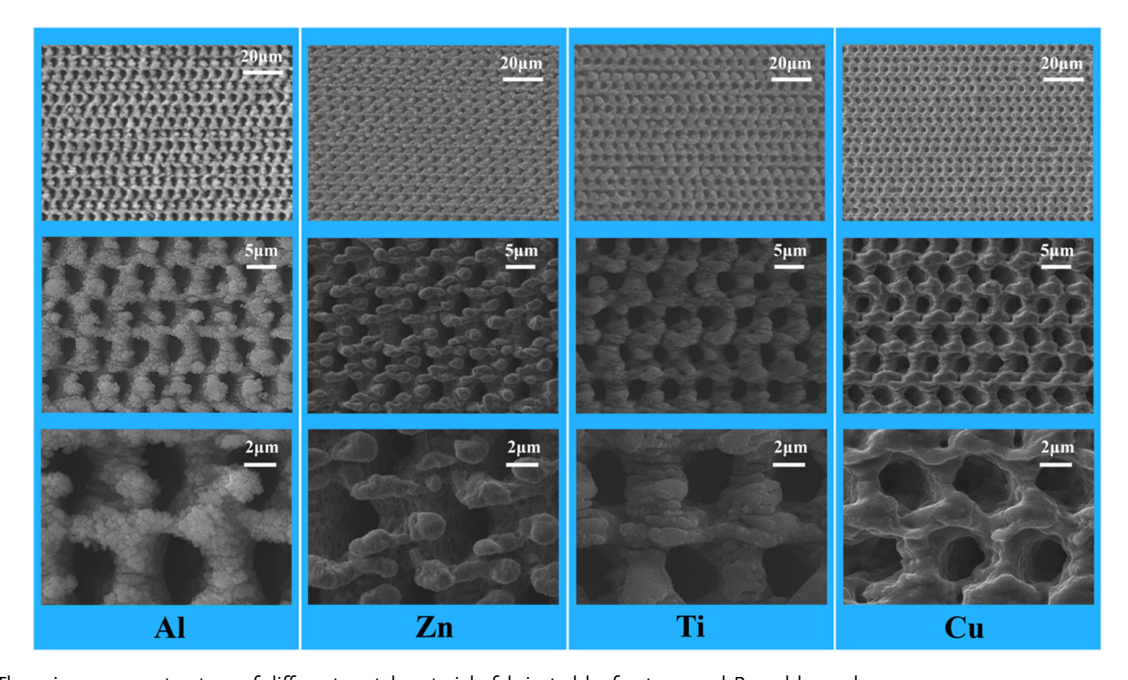


Figure 5. The microporous structure of different metal materials fabricated by femtosecond Bessel beam laser.

15272648, 2022, 10, Downloaded from https://advanced.onlinelibrary.wiley.com/doi/10.1002/adem.202101738 by CAS-XIAN INSTITUTION OPTICS PRECISION MECHANICS, Wiley Online Library on [1011/1025]. See the Terms and Conditions (https://onlinelibrary.wiley.com/dem.

and-conditions) on Wiley Online Library for rules of use; OA articles are governed by the applicable Creative Commons License.

www.advancedsciencenews.com www.aem-journal.com

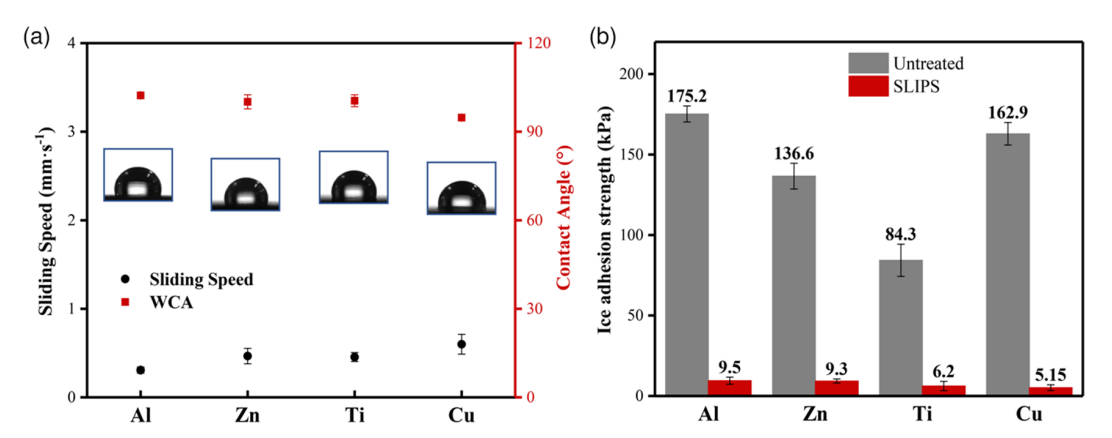


Figure 6. a) WCA and sliding speed on untreated surface and SLIPS of different metal substrates, b) ice adhesion test on untreated surface and SLIPS of different metal substrates.

each SLIPS is measured three times and averaged shown at the black point in Figure 5a. The sliding speeds of SLIPS of Al, Zn, Ti, Cu are 0.308, 0.466. 0.455, 0.599 mm s<sup>-1</sup>, respectively. The SLIPS exhibits excellent ice adhesion resistance of 5.15–9.5 kPa as shown in Figure 6b, which reduced ice adhesion by two orders of magnitude relative to the intrinsic surface of Al, Zn, Ti, Cu substrate. Thus, the SLIPS can be realized on various metal materials by this method, which has a great potential to meet different ice restraint applications.

# 3. Conclusions

In conclusion, we developed a versatile, one-step way to form microporous on many different types of metal materials including stainless steel, Al, Zn, Ti, Cu. The microporous structure was induced by femtosecond Bessel beam pulse on substrate surface through adjusting the processing parameters. SLIPS would be prepared with chemical treatment of the porous surface for lowering the surface free energy followed by the infusion of a lubricating liquid. As a representative, SLIPS based on stainless steel shows a great performance of liquid repellency, ice resistance, and durability. SLIPS preserves great ice restraint properties, with an ice-delay time of SLIPS was extended by 21.5% and 43.3% compared to SHS and untreated surface at a temperature of -30 °C, and the ice-adhesion strength can remain below 15 kPa after being repeated several times. After different harsh environmental tests including hydraulic pressure of 30 meters, high- and low-temperature cycle (130--30 °C), salt fog test with a condition of 5 wt% NaCl fog at 35 °C for 2 days, the SLIPS sliding velocity has little change and maintained great liquid repellency. The SLIPS was processed on Al, Zn, Ti, Cu by using the same method, all the SLIPS exhibits the prominent performance of liquid resistance and ice-adhesion resistance. Therefore, the femtosecond Bessel beam laser induce method can be used to enable almost all hard metal materials to become a substrate of choice for constructing SLIPS. The excellent anti-icing performance of SLIPS provides a broad application prospect with different types of substrate materials.

# 4. Experimental Section

The SLIPS sample was made by 304 stainless steel plate, which was purchased from the local metal store (China), the other mental plates were purchased from the local metal store (China) as well. The 304 stainless plates were first polished by sandpapers (#600, #1000, #2000, and #4000 in sequence) to make the surface of the sample highly smooth for laser objective focusing, followed by a thorough cleaning with deionized water and ethanol, respectively. Then, the femtosecond Bessel beam laser was conducted to obtain porous structure, the femtosecond laser source used a fiber laser machine (Femto YL-40, YSLP). The original femto second laser pulses (pulses width of 400 fs; central wavelength of 1030 nm; fundamental frequency of 5 MHz) were adjusted by an external trigger (the select-frequency of 3 kHz, the duty ratio of 25%, the original laser power of 3.45 W). The femtosecond Bessel laser beam was produced from Gaussian beam by through an axicon (Thorlabs, AX-250,  $\alpha$  of 1°), then focused on the surface of stainless steel (China Baowu Steel Group) by an objective lens ( $\times$ 20, NA = 0.40, Nikon) on a moveable platform to proceed the ablation process (laser canning speed =  $15 \text{ mm} \cdot \text{s}^{-1}$ , the scanning interval of 5 µm). After that, a fluoroalkylsilane modification was conducted by immersing the sample into fluorosilane (1H, 1H, 2H, 2H) alcohol solution (0.05 wt%) for 12 h, then heating (120 °C) for 2 h, and in this way, the sample surface would have superhydrophobic properties. To prepare SLIPSs, the silicone oil (200 mPa s at 25 °C) was dropped onto the tilted sample that we prepared before, then wait for the silicon oil to slowly fill the sample's pores.

A SEM, FlexSEM-1000 Hitachi, Japan, was used to characterize the morphology of the prepared samples. An optical contact angle measuring device (JC2000D, PowerReach, China) was used to measure the WCA, sliding angle (SA). A homemade device was utilized to measure the ice adhesion strength. An ice cubic was formed in a colorimetric dish  $(10 \times 10 \times 10 \text{ mm}^3)$  on the sample (temperature of  $-30 \pm 1\,^{\circ}\text{C}$  for at least 7 h). A force gauge (HP-50, HANDPI, China) was then used to record the deicing force during the process of removing the ice blocks. To demonstrate the durability of the SLIPS, the sliding speed of water droplets were studied on the tilted surface (title angle =  $10^{\circ}$ ) after salt fog (YX-YW-60L, YUEXIN, China), hydraulic pressure test (YX-JL-QF30-40L, YUEXIN, China), high ( $130\,^{\circ}\text{C}$ ) and low ( $-30\,^{\circ}\text{C}$ ) temperature transformation under constant humidity (KCSHWHS, AISRY, China), respectively.

# **Supporting Information**

Supporting Information is available from the Wiley Online Library or from the author.

www.advancedsciencenews.com

www.aem-journal.com

, 2022, 10, Downloaded from https://advanced.onlinelibrary.wiley.com/doi/10.1002/adem.202101738 by CAS-XIAN INSTITUTION OPTICS PRECISION MECHANICS, Wiley Online Library on [10/11/2025]. See the Terms

# Acknowledgements

This work is supported by the National Science Foundation of China under the Grant nos. 61875158, 62175195, the National Key Research and Development Program of China under grant no. 2017YFB1104700, the International Joint Research Laboratory for Micro/Nano Manufacturing and measurement Technologies, the Fundamental Research Funds for the Central Universities.

# Conflict of Interest

The authors declare no conflict of interest.

# **Data Availability Statement**

The data that support the findings of this study are available from the corresponding author upon reasonable request.

# **Keywords**

anti-icing, femtosecond laser, metal materials, SLIPS, water repellency

Received: January 17, 2022 Revised: February 19, 2022 Published online: March 27, 2022

- S. Lei, F. Wang, X. Fang, J. Ou, W. Li, Surf. Coat. Technol. 2019, 363, 362.
- [2] Y. Liu, L. Ma, W. Wang, A. K. Kota, H. Hu, Appl. Surf. Sci. 2018, 447, 599.
- [3] H. Hu, J. Wen, L. Bao, L. Jia, D. Song, B. Song, G. Pan, M. Scaraggi, D. Dini, Q. J. S. A. Xue, Sci. Adv. 2017, 3, 1603288.
- [4] C. Zhu, S. Liu, Y. Shen, J. Tao, G. Wang, L. Pan, Surf. Coat. Technol. 2017, 309, 703.
- [5] M. Huneault, C. Langheit, R. S. Arnaud, J. Benny, J. Audet, J. C. Richard, IEEE Trans. Power Delivery 2005, 20, 1604.
- [6] X. Jiang, C. Fan, Y. Xie, IET Gener. Transm. Distrib. 2019, 12, 536.
- [7] W. Zhou, J. C. Chan, W. Chen, J. Ling, J. G. Pinto, Y. Shao, Min, Weather. Rev. 2009, 137, 3978.
- [8] Z. Hao, J. Zheng, Q. Ge, Clim. Res. 2011, 50, 161.
- [9] J. Wang, IEEE Trans. Power Delivery 2012, 27, 1234.
- [10] X. Jiang, S. Wang, Z. Zhang, S. Xie, Y. Wang, IEEE Trans. Power Delivery 2007, 22, 472.
- [11] Y. Liu, G. Li, J. Colloid Interface Sci. 2012, 388, 235.
- [12] R. Fürstner, W. Barthlott, C. Neinhuis, P. Walzel, Langmuir 2005, 21, 956.
- [13] H. Zhang, J. Tan, Y. Liu, C. Hou, Y. Ma, J. Gu, B. Zhang, H. Zhang, Q. Zhang, Mater. Des. 2017, 135, 16.
- [14] D. Zhang, C. Feng, G. Fang, Q. Yang, D. Xie, G. Qiao, W. Li, J. Si, X. Hou, J. Micromech. Microeng. 2010, 20, 075029.

- [15] J. Yong, Q. Yang, C. Guo, F. Chen, X. Hou, RSC Adv. 2019, 9, 12470.
- [16] A. Pan, B. Gao, T. Chen, J. Si, C. Li, F. Chen, X. Hou, Opt. Express 2014, 22, 15245.
- [17] J. C. Bird, R. Dhiman, H. M. Kwon, K. K. Varanasi, *Nature* 2013, 503, 385.
- [18] Y. Shen, G. Wang, J. Tao, C. Zhu, S. Liu, M. Jin, Y. Xie, Z. Chen, Adv. Mater. Interfaces 2017, 4, 1700836.
- [19] Y. Liu, M. Andrew, J. Li, J. M. Yeomans, Z. Wang, Nat. Commun. 2015, 6, 10034.
- [20] Y. Liu, X. Yan, Z. Wang, Biosurf. Biotribol. 2019, 5, 35.
- [21] Y. Shen, H. Tao, S. Chen, L. Zhu, T. Wang, J. Tao, RSC Adv. 2015, 5, 1666.
- [22] H. Sojoudi, M. Wang, N. D. Boscher, G. H. McKinley, K. K. Gleason, Soft Matter 2016, 12, 1938.
- [23] J. Yong, F. Chen, J. Huo, Y. Fang, Q. Yang, H. Bian, W. Li, Y. Wei, Y. Dai, X. Hou, ACS Omega 2018, 3, 1395.
- [24] J. Yong, F. Chen, Q. Yang, D. Zhang, H. Bian, G. Du, J. Si, X. Meng, X. Hou, *Langmuir* 2013, 29, 3274.
- [25] J. Yong, F. Chen, Q. Yang, X. Hou, Soft Matter 2015, 11, 8897.
- [26] J. Yong, F. Chen, Y. Fang, J. Huo, Q. Yang, J. Zhang, H. Bian, X. Hou, ACS App. Mater. Interfaces 2017, 9, 39863.
- [27] J. Yong, Q. Yang, X. Hou, F. Chen, Nanomaterials 2022, 12, 688.
- [28] J. Yong, Q. Yang, J. Huo, X. Hou, F. Chen, Int. J. Extreme Manuf. 2022, 4, 015002.
- [29] H. Wang, M. He, H. Liu, Y. Guan, ACS Appl. Mater. Interfaces 2019, 11, 25586.
- [30] X. He, P. Cao, F. Tian, X. Bai, C. Yuan, Surf. Coat. Technol. 2019, 358, 159
- [31] S. Heydarian, R. Jafari, G. Momen, *Prog. Org. Coat.* **2021**, *151*, 106096
- [32] C. H. Xue, J. Z. Ma, J. Mater. Chem. A 2013, 1, 4146.
- [33] T. Verho, C. Bower, P. Andrew, S. Franssila, O. Ikkala, R. H. Ras, Adv. Mater. 2011, 23, 673.
- [34] W. Li, Y. Zhan, S. Yu, Prog. Org. Coat. 2021, 152, 106117.
- [35] T. S. Wong, S. H. Kang, S. K. Y. Tang, E. J. Smythe, B. D. Hatton, A. Grinthal, J. Aizenberg, *Nat. Cell Biol.* 2011, 477, 443.
- [36] J. Kamei, H. Yabu, Adv. Func. Mater. 2015, 25, 4195.
- [37] C. Liu, Y. Li, C. Lu, Y. Liu, S. Feng, Y. Liu, ACS Appl. Mater. Interface 2020, 12, 25471.
- [38] S. Barthwal, B. Lee, S. Lim. Appl. Surf. Sci. 2019, 496, 143677.
- [39] S. Anand, A. T. Paxson, R. Dhiman, J. D. Smith, K. K. Varanasi, ACS Nano 2012, 6, 10122.
- [40] P. Kim, T. S. Wong, J. Alvarenga, M. J. Kreder, W. E. Adorno-Martinez, J. Aizenberg, ACS Nano 2012, 6, 6569.
- [41] F. L. Heale, I. P. Parkin, C. J. Carmalt, ACS Appl. Mater. Interfaces 2019, 11, 41804.
- [42] J. Yong, J. Huo, Q. Yang, F. Chen, Y. Fang, X. Wu, L. Liu, X. Lu, J. Zhang, X. Hou, Adv. Mater. Interfaces 2018, 5,1701479.
- [43] H. Luo, Y. Lu, S. Yin, S. Huang, J. Song, F. Chen, F. Chen, C. J. Carmalt, I. P. Parkin, J. Mater. Chem. A 2018, 6, 5635.
- [44] Y. Cheng, Q. Yang, Y. Lu, J. Yong, Y. Fang, X. Hou, F. Chen, Biomater. Sci. 2020, 8, 6505.

articles are governed by the applicable Creative Commons License